buildings

Article

Mechanical Properties and Absorption of High-Strength Fiber-Reinforced Concrete (HSFRC) with Sustainable Natural Fibers

Muttaqin Hasan *, **Taufiq Saidi**, **Muhammad Jamil**, **Zahra Amalia** and **Azzaki Mubarak**

Department of Civil Engineering, Universitas Syiah Kuala, Banda Aceh 23111, Indonesia
* Correspondence: muttaqin@unsyiah.ac.id

Abstract: This study aimed to determine the mechanical properties and absorption of high-strength fiber-reinforced concrete (HSFRC), using sustainable natural fibers. In this analysis, two types of fibers were used, namely, ramie and abaca. Two different HSFRC mixtures were also designed, where one composition emphasized ordinary Portland cement (OPC) as a binder, and the other prioritizing calcined diatomaceous earth (CDE) as a mineral additive to replace 10% weight of OPC. Furthermore, ramie and abaca fibers were separately added to the mixtures at three different volumetric contents. Based on the results, the addition of these fibers in the concrete mixtures improved the mechanical properties of HSFRC. The improvements of compressive strength, splitting tensile strength, and flexural strength, due to the addition of ramie fiber were 18%, 17.3%, and 31.8%, respectively, while those for the addition of abaca fiber were 11.8%, 17.2%, and 38.1%, respectively. This indicated that the fibers were capable of being used as alternative materials for sustainable concrete production. The effects of ramie and abaca fibers on the absorption of HSFRC were also not significant, and their presence for the same amount of superplasticizer reduced the flow speed of fresh reinforced concrete mixtures.

Keywords: ramie fiber; abaca fiber; high-strength fiber reinforced concrete; mechanical properties; absorption; flow speed

Citation: Hasan, M.; Saidi, T.; Jamil, M.; Amalia, Z.; Mubarak, A. Mechanical Properties and Absorption of High-Strength Fiber-Reinforced Concrete (HSFRC) with Sustainable Natural Fibers. *Buildings* **2022**, *12*, 2262. https://doi.org/10.3390/buildings12122262

Academic Editor: Abdelhafid Khelidj

Received: 15 November 2022
Accepted: 15 December 2022
Published: 19 December 2022

1. Introduction

High-strength concrete (HSC) is a material with a compressive strength above 55 MPa [1]. Due to high cement use in producing HSC, some binders are often replaced with supplementary cementitious materials (SCMs) [2–4]. In this process, a pozzolanic reaction is expected between silica in SCMs and calcium hydroxide, which is a product of the cement hydration. This often leads to the formulation of more calcium silicate hydrate, which enables the continuous development of HSC strength with the increasing age of concrete [5]. The use of SCMs is also expected to increase the durability of concrete [6–9]. From this context, an SCM used for the production of high-strength concrete is calcined diatomaceous earth (CDE) [10–12], which is part of natural pozzolanic materials [13].

The use of fibers in HSC mixtures has reportedly been practiced for quite a long time [14–16], with the resulting composition, known as high-strength fiber-reinforced concrete (HSFRC). The main purpose of these fibers being added is to increase the tensile strength of the mixtures [17–19], because concrete has low tensile strength, although it has high strength [20–24]. The addition of fibers also aims to increase the fracture strain capacity, control cracks, anticipate brittle properties, elevate concrete ductility and toughness, as well as develop resistance to crack opening [25–27]. Furthermore, the use of fibers in the HSFRC mixtures enhances durability and early-age properties, such as reducing drying shrinkage and early-age cracking [28–35]. The fiber content, as well as its type, orientation, geometry, and density, subsequently affect the mechanical properties of HSFRC [36,37]. In this process, synthetic fibers, such as steel, glass, and polypropylene, are often provided to HSFRC mixtures [38–43]. Regarding these fiber types, the polypropylene material is the only environmentally friendly component solely emitting 78 kg of CO_2 per ton of production [44]. Meanwhile, the CO_2 emission in the steel fiber analysis is quite high, at approximately 1600 kg per ton of production, and, thus, becoming an environmentally unfriendly material [45]. For the overall glass process, the emission of CO_2 is also 490 kg per ton of production [46].

In the production of more environmentally friendly cement-based material, many previous studies were carried out on natural fibers [47–52], such as jute, coir, sisal, bamboo, and hemp [48–50,53–55]. For example, the addition of 2% coir fiber increased the splitting tensile, flexural, and compressive strengths (STS, FS, and CS) by 9.46–11.29%, 10.62–15.52%, and 10.34–15.20%, respectively [54,55]. In the addition of 2% jute fiber, the STS, FS, and CS were also increased by 7.66%, 12.07%, and 13.68%, respectively [54]. Meanwhile, the addition of sisal fiber at 2% concrete volume increased the STS, FS, and CS by 9.00%, 13.79%, and 14.18%, respectively [54]. The addition of these natural fibers also improved ductility, impact resistance, toughness, and drying shrinkage, although it reduced concrete durability [54,56].

Ramie and abaca fibers are two material types obtained from plants. In the preparation of ramie fiber, the stems of the ramie (Boehmeria nivea) plants were extracted for analyses in [57–59], with the final products often used as textile materials, such as clothing, table cloths, handkerchiefs, paper, cordage, gas mantles, fishing nets, etc. [60]. They are also used as biomedical products, automobile parts, industrial materials, etc. [61]. Meanwhile, abaca fiber is obtained from the trunk of a banana plant (Musa textilis NEE) indigenous to the Philippines [62]. This material is often used to produce fiber-reinforced polymer composites, due to its high tensile strength [63–68]. These descriptions indicate that no reports have been conducted to determine the increase in the mechanical properties of HSFRC with the addition of ramie and abaca fibers. Since these materials are obtained from plants (renewable materials), they are classified as sustainable natural fibers. They are also classified as environmentally friendly materials, due to their low emission of CO_2 into the atmosphere during their manufacturing processes. Therefore, this study aimed to determine the mechanical properties and absorptions of HSFRC using sustainable natural fibers.

In this analysis, two kinds of HSFRC mixtures using cement and CDE as a binder and partial cement substitution were studied, respectively. Ramie and abaca fibers at three different volumetric contents were added to both mixtures, separately. The flow of fresh concrete and mechanical properties of hardened concrete, including compressive, flexural, and splitting tensile strengths were then evaluated. The results were expected to enhance the use of ramie and abaca fibers as alternative materials in the HSFRC mixtures. This, subsequently, led to the production of environmentally friendly concrete and enforcement of HSFRC production sustainability. In addition, changes were presented in the absorption of HSFRC, due to the provision of ramie and abaca fibers. The ability of concrete to absorb liquid is closely related to the ingress of aggressive fluids, gases, and ions from the external environment which determines its durability properties.

2. Materials and Methods

2.1. Materials

The materials used in this study consisted of cement, diatomaceous earth, aggregates, fibers, water, and superplasticizer.

2.1.1. Cement

A Type-I Ordinary Portland Cement (OPC), produced by PT. Semen Padang, was used, which met the requirements of ASTM C150/C150M-22 [69]. The physical properties of this material are shown in Table 1. Its particle size distribution was also examined by testing with a Particle Size Analyzer (PSA) through a MicroBrook 2000 L instrument, with the results shown in Figure 1. Furthermore, the chemical composition of OPC was analyzed by an XRF test, using the XRF Analyzer of TORONTOTECH TT-EDXPRT.XRF. In this case, the chemical composition obtained is shown in Table 2.

Table 1. Physical properties of OPC and CDE.

Binder	Specific Gravity	Absorption (%)	Specific Surface Area (m^2/kg)	Fineness Characteristics		
				d20 (μm)	d50 (μm)	d80 (μm)
OPC	3.15	NA	539.80	2.42	10.62	34.20
CDE	2.00	6.54	675.60	5.42	18.35	38.69

Note: d20 = the particle size with a cumulative finer of 20%; d50 = the particle size with a cumulative finer of 50% (median particle size), and d80 = the particle size with a cumulative finer of 80%.

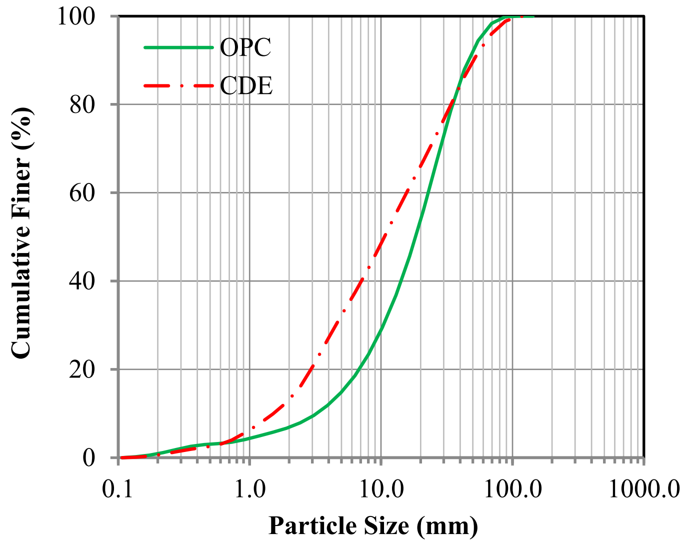

Figure 1. Particle size distribution of OPC and CDE.

Table 2. Chemical composition of OPC and CDE.

Chemical Composition	OPC (%)	CDE (%)
SiO_2	17.25	78.73
Al_2O_3	2.32	0.39
Fe_2O_3	4.67	2.89
MgO	2.13	1.11
SO_3	2.56	0.39
CaO	70.34	16.34
K_2O	0.73	0.15

2.1.2. Diatomaceous Earth

Diatomaceous earth is used as a mineral additive to partially replace cement, which is also a binder. This additive was obtained in lumps from Beureunuet Village, Aceh Besar District, Indonesia. These collections emphasized the data released by the Aceh Provincial Mining and Industry Service, where the diatomaceous earth deposits in the village reached 40,353,700 tons [70–72]. The material was oven-dried at 100 °C for 24 h, mashed, and sieved through a #200 sieve. The powder passing through this filter was then calcined in a furnace, at a temperature of 500 °C for 5 h. The physical properties and the PSA outcomes of the calcined diatomaceous earth (CDE) are shown in Table 1 and Figure 1, respectively. Based on Figure 1, the CDE had finer particles than OPC. The XRD pattern of CDE, tested using a Maxima XRD-7000 device manufactured by SHIMADZU, is shown in Figure 2. The result indicated that silica (quartz), graphite, and rayite were the main crystalline minerals. An XRF test was also carried out on CDE, and the results shown in Table 2. In this process, the main composition of CDE was silica (SiO_2) which reached 78.73%. This was then used as a mineral additive to partially replace cement. The CDE was also tested using a microphotograph through Scanning Electron Microscopy (SEM), and the results are shown in Figure 3. This indicated that the CDE particles had cylindrical shapes with cellular structures of about 2 μm in diameter.

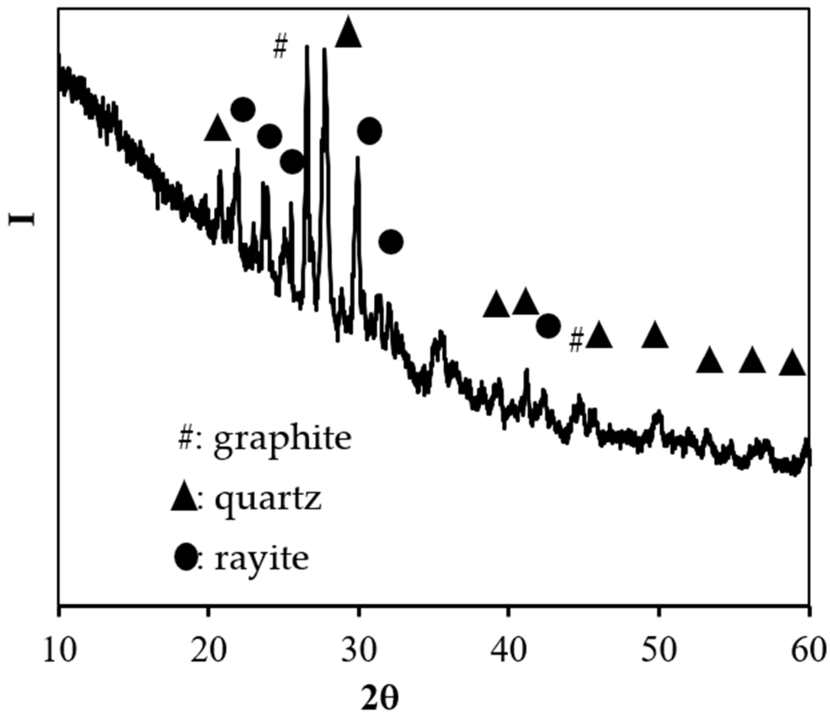

Figure 2. XRD pattern of CDE.

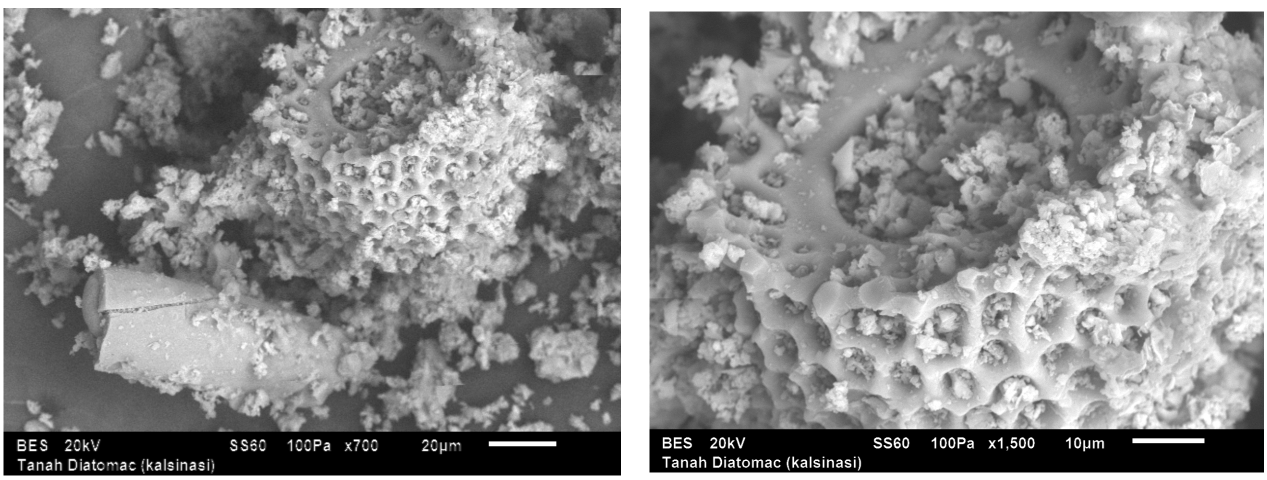

Figure 3. Microphotograph of CDE.

2.1.3. Aggregates

Two types of aggregates were used in this study, namely, fine and coarse. We used river sand (RS) and split stone (SS) with maximum diameters of 2.36 and 9.52 mm, respectively. The sand and stones used originated from the Krueng Aceh River and the stone-crushing industry in Aceh Besar District, respectively. The specific gravity and gradation of these aggregates are shown in Table 3 and Figure 4. It was proved that they met the requirements of concrete aggregates, according to ASTM C33/C33M-18 standard [73].

Table 3. Physical properties of aggregates.

Type of Aggregate	Bulk Density (kg/m^3)	Specific Gravity		Absorption (%)	Fineness Modulus
		Saturated Surface Dry	Oven Dry		
RS	1.62	2.70	2.65	1.87	3.37
SS	1.41	2.80	2.78	0.66	5.70

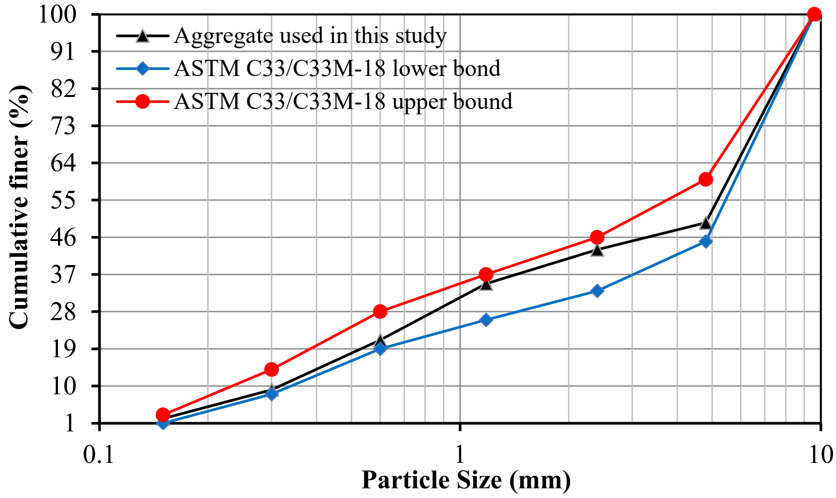

Figure 4. Gradation of aggregates and comparison with ASTM C33/C33M-18 requirements.

2.1.4. Fibers

In this analysis, two types of fibers were used, namely, ramie (RF) and abaca (AF), which were obtained from Central Java. Before being used in the concrete mix, these materials were initially cut to fiber lengths (L), with aspect ratios (L/D) of 100. Figures 5 and 6 show the ramie and abaca fibers before and after cutting, respectively. Moreover, fiber diameters were measured using digital calipers, as shown in Figure 7. Tensile tests were also carried out on these materials using a universal testing machine (Shimadzu AGS-X series), with a capacity of 5 kN, to determine the strength, elasticity modulus, and ultimate strain. In accordance with the ASTM D3822/D3822M-14 [74] standard, the fiber tensile test was carried out as shown in Figure 8, with the physical and mechanical properties of the two materials observed in Table 4.

Figure 5. Ramie fiber before and after cutting.

Figure 6. Abaca fiber before and after cutting.

Figure 7. Measurement of rami fiber diameter.

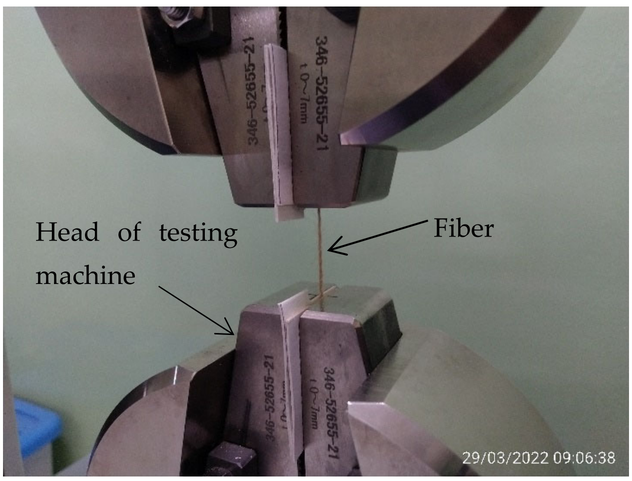

Figure 8. Tensile test of fiber.

Table 4. Physical and mechanical properties of fibers.

Type of Fiber	Diameter (mm)	Length (mm)	L/D	Specific Gravity	Tensile Strength (MPa)	Ultimate Strain (%)
RF	0.09	9	100	1.44	282.09	5.46
AF	0.17	17	100	1.50	1760.22	3.75

2.1.5. Water

Clean drinkable water, supplied by the PDAM (Regional Water Company), was used for the mixture of the concrete, meeting the requirements for water-mixed materials in ASTM C1602/C1602M-22 [75].

2.1.6. Superplasticizer

A polycarboxylate-based superplasticizer, produced by PT. Sika Indonesia, was used to improve concrete workability, with the specific gravity being 1.06.

2.2. Method

2.2.1. Mixture Proportion

The mixture proportion of HSFRC was determined, based on ACI 211.4R-93 [76], using a water-to-binder ratio (w/b) of 0.27. The initial step was to determine the mixture proportion without additional fiber and use of CDE (coded HSC00F00). This proportion was, subsequently, used as a control mixture. Furthermore, 10% of the OPCs in the HSC00F00 mixture were replaced with CDE and coded HSC10F00. We used10% CDE because previous studies showed that the maximum compressive strength was reached with a CDE content of 10% [10,69]. Ramie and abaca fibers were then added to these two mixtures, HSC00F00 and HSC10F00, with 0.15%, 0.3%, and 0.45% of the total volume of concrete. This, subsequently, led to the total collection of 14 different mixtures. For 1 m^3 of concrete volume, the proportion of all HSFRC mixtures is shown in Table 5. In this case, the mixture code values emphasized the number of CDEs used to replace OPC and fiber content. For example, HSC10RF15 used 0.15% of ramie fiber and 10% CDE as cement replacement.

Table 5. Mixture proportion for 1 m^3 HSFRC.

Mixture	CDE Content (% Binder Weight)	Fiber Content (% Concrete Volume)	OPC (kg)	CDE (kg)	RS (kg)	SS (kg)	Water (kg)	SP (kg)	RF (kg)	AF (kg)
HSC00F00	0	0	758.31	0.00	565.15	901.72	205.05	11.37	-	-
HSC10F00	10	0	682.48	75.83	565.15	901.72	205.05	11.37	-	-
HSC00RF15	0	0.15	758.31	0.00	565.15	901.72	205.05	11.37	2.16	-
HSC00RF30	0	0.30	758.31	0.00	565.15	901.72	205.05	11.37	4.32	-
HSC00RF45	0	0.45	758.31	0.00	565.15	901.72	205.05	11.37	6.48	-
HSC00AF15	0	0.15	758.31	0.00	565.15	901.72	205.05	11.37	-	2.25
HSC00AF30	0	0.30	758.31	0.00	565.15	901.72	205.05	11.37	-	4.50
HSC00AF45	0	0.45	758.31	0.00	565.15	901.72	205.05	11.37	-	6.75
HSC10RF15	10	0.15	682.48	75.83	565.15	901.72	205.05	11.37	2.16	-
HSC10RF30	10	0.30	682.48	75.83	565.15	901.72	205.05	11.37	4.32	-
HSC10RF45	10	0.45	682.48	75.83	565.15	901.72	205.05	11.37	6.48	-
HSC10AF15	10	0.15	682.48	75.83	565.15	901.72	205.05	11.37	-	2.25
HSC10AF30	10	0.30	682.48	75.83	565.15	901.72	205.05	11.37	-	4.50
HSC10AF45	10	0.45	682.48	75.83	565.15	901.72	205.05	11.37	-	6.75

2.2.2. Specimen Preparation

To develop a concrete mixture, all solid materials, namely aggregates, OPC, and CDE, were placed into a mixer and stirred for approximately 3 min until evenness was achieved. This was accompanied by the provision of water and superplasticizer to the concrete mixer, which was repeatedly stirred for approximately 3 min until all mixtures were evenly composed. Moreover, the fiber was added to the mixture, with the mixer continuously rotated and stirred for about 4 min. In this process, all the fibers were evenly distributed into the concrete mix.

Specimens were developed by pouring the concrete mixture into the mold provided. These were then compacted by tapping the external part of the mold with a rubber mallet. For compression and split tensile testing, cylindrical specimens, with a diameter and height of 100 mm and 200 mm, were developed, respectively. Meanwhile, the samples were developed as a beam with a size of 100 × 100 × 400 mm for flexural analysis. Based on the tests, 5 specimens were developed for each HSFRC mixture. The mold was also opened for subsequent curing when the age of the specimens reached 24 h. This was carried out by immersing the molds in clean water in an immersion bath for 27 days. After reaching the age of 28 days, the specimens were then removed from the bath and dried, for subsequent analysis of mechanical properties and absorption. Some photos of specimen preparation are shown in Figure 9.

(**a**) (**b**) (**c**)

(**d**) (**e**) (**f**)

Figure 9. Photos of specimen preparation: (**a**) mixing; (**b**) casting; (**c**) leveling; (**d**) after casting; (**e**) mold removing; and (**f**) curing.

2.2.3. Flow Test

Before the specimens were cast into the mold, a flow test was initially performed on the fresh concrete, using Abram's cones. These cones were placed upside down on a steel plate, with a small diameter side located at the bottom. On this plate, a circle with a diameter of 50 cm was initially designed. Furthermore, the cones were placed in the middle of the circle and inserted into the concrete mixture in 3 layers. In this process, each layer was filled with one-third of the cone height and pierced with an iron rod 25 times. After filling, the top surface was then leveled with a cement spoon and the cone was lifted, leading to the sideways flow of the concrete mixture. Since the flow reached a diameter of 50 cm in the previously marked circle, the time taken for the cone to be lifted was conducted using a stopwatch. The flow speed was also obtained through the division of the diameter (50 cm) by the travel time measured by the stopwatch.

2.2.4. Compression Test

The compression test was carried out using a universal testing machine (Ton Industry) with a capacity of 100 tons, according to the ASTM C39/C39M-21 standard [77]. In this process, the cylindrical specimen was placed on the base of the machine, with the load applied at a speed of 0.25 MPa/s until the destruction of the sample. When crushed, the maximum load was then recorded, with the compressive strength obtained in its division by the cross-sectional area of the cylinder.

2.2.5. Flexural Test

The flexural test was conducted using a universal testing machine (Mohr & Federhaff AG) with a capacity of 10 tons, according to the ASTM C78/C78M-22 standard [78], through the insertion of the beam specimen on two supports, with the beam span being 300 mm. Two-point loads were also applied to the upper side of the beam, with the force–distance from the support being 100 mm. The load was then applied at a speed of 0.90 MPa/min until fracturing of the specimen. These conditions were appropriately recorded and accompanied by the calculation of flexural strength.

2.2.6. Splitting Tensile Test

This analysis was carried out using a universal testing machine (Ton Industry) with a capacity of 100 tons, and according to the ASTM C496/C496M-17 standard [79]. The specimen was placed on the base of the testing machine, with the laid plywood having a thickness of 3.2 mm. The load was then applied through the upper side of the cylindrical blanket until the specimen was divided into two parts. The magnitude of the maximum load was also recorded for the subsequent calculation of splitting tensile strength (STS).

2.2.7. Absorption Test

The absorption test was conducted based on the ASTM C642–21 standard [80]. A cube with a side of 50 mm was used. This specimen was obtained by cutting the remaining samples from the flexural test. For each HSFRC mixture, 5 specimens were prepared for this test and oven-dried at 100 °C for 24 h. After this process, the weights of these samples were remeasured and re-baked in the oven at 100 °C for 24 h. This was performed until the weights were constant, indicating that no pore water was available in the concrete. Moreover, the specimens were immersed in water and weighed every 5 min for the first 30 min of immersion. This was then accompanied by the measurement of the weight change at every 10 min of immersion for 60 min. Subsequent analyses were also conducted every 15 min and 2 h of immersion for 120 min and 24 h, respectively. When the weight change was no longer present after 24 h of immersion, the ratio of the transformation to the initial mass of the specimen became the absorption of the HSFRC (%). However, the immersion process was continuously carried out for more than 24 h, due to the persistence of the weight change. This was repeatedly conducted until changes were no longer observed in the sample mass.

3. Results and Discussion

3.1. Flow

Figures 10 and 11 show the flow speed of fresh HSFRC, using ramie and abaca fibers, respectively. Based on the results, the presence of 10% CDE, as a cement replacement, reduced the flow speed of HSFRC. This indicated that the mixture workability was lower when using CDE as cement replacement, compared to others with only OPC. These results were in line with the nature of CDE, which absorbed water at 6.54% (Table 1). The high absorption level of this material also caused the immersion of some water into its pores. This proved that the mixing water level and the flow value of the CDE-based mixture were reduced. Regarding Figure 1 and Table 1, CDE had finer particles than OPC. This was explained by the fact that it had a larger surface area than OPC for the same amount of material. These conditions caused more wetness of the CDE surface than that of the OPC, leading to a decrease and increase in the required levels of free and mixing water, respectively [81–83]. When the level of water and superplasticizer used for all mixtures was similar, a lower flow of CDE-based HSFRC composition was observed.

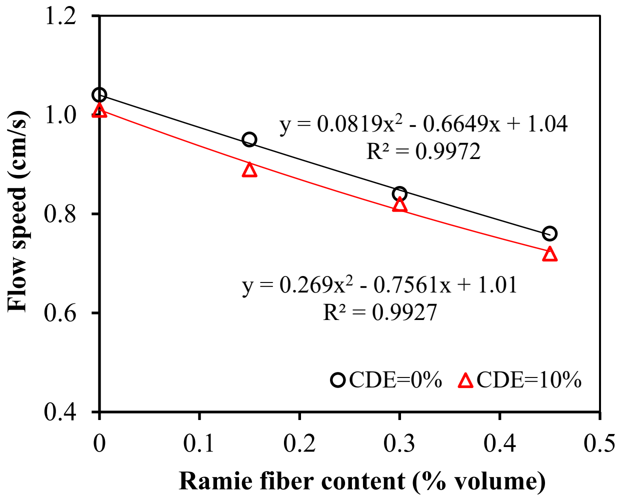

Figure 10. The flow speed of fresh HSFRC with ramie fiber.

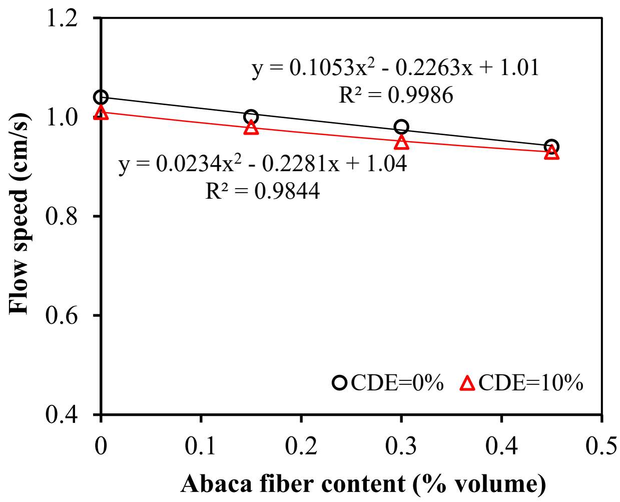

Figure 11. The flow speed of fresh HSFRC with abaca fiber.

Based on Figures 10 and 11, the flow speed of the fresh HSFRC mixture decreased as the volumetric content of ramie and abaca fibers increased. This showed that the shapes of these fibers were longer than those of the aggregates. For similar volumes, larger surface areas were also observed for the fibers than the aggregates. This confirmed that the addition of fibers to the concrete mix increased the cohesive forces between the fibers and the cement matrices [84]. These conditions impeded the flow of the concrete mixture, proving that the speed decreased with increased fiber estimations. Similar results were also reported for the use of fiber in normal-strength and ultra-high-performance concrete [85–87]. Regarding these results, the reduction in ramie-based flow speed was greater than that of the abaca-based speed.

3.2. Compressive Strength

Figures 12 and 13 show the compressive strength test of the HSFRC mixtures with and without CDE, using ramie and abaca fibers. These results proved that the addition of 0.15% ramie or abaca fibers significantly increased the compressive strength of the mixtures. Based on the addition of 0.15% ramie fiber (RF), the compressive strength (CS) increased by 18% and 9.4% for the HSFRC without and with CDE, respectively. CS then decreased for the addition of 0.3% RF volume, although the value was greater than that of the concrete without a fibrous material. Meanwhile, the addition of 0.45% RF produced a compressive strength smaller than the non-fibrous concrete. This indicated that the increase and decrease in the CS of ramie-based HSFRC had a parabolic tendency.

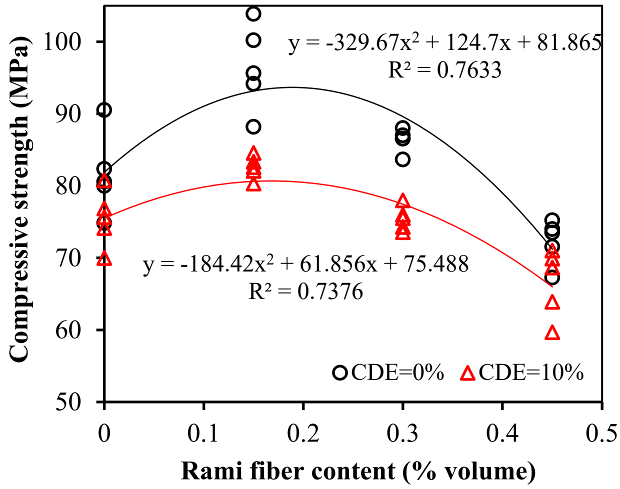

Figure 12. Compressive strength of HSFRC with ramie fiber.

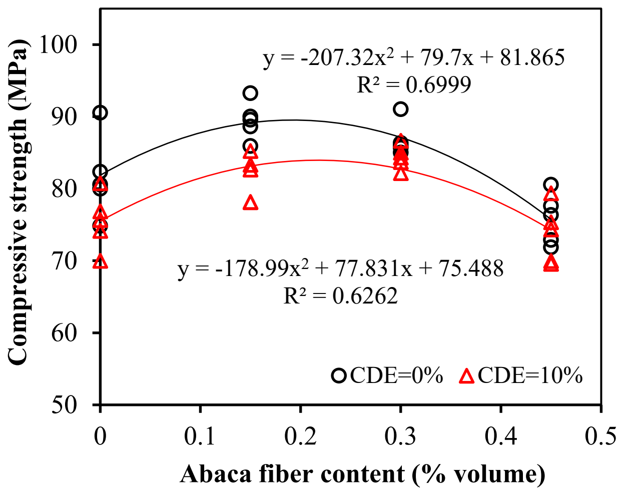

Figure 13. Compressive strength of HSFRC with abaca fiber.

Regarding the addition of 0.15% abaca fiber (AF), the compressive strength increased by 9.6% for the HSFRC without CDE. Similar to the use of ramie fiber, the addition of 0.3% AF caused decreased CS, although the value was greater than that of the non-fibrous concrete. However, the addition of 0.45% AF produced a smaller compressive strength than fiber-free concrete. In the CDE-based HSFRC, serving as a substitute for 10% OPC, the CS increased and decreased with the additions of 0.3% and 0.45% AF, respectively. In this process, the highest compressive strength was found at the 0.3% volumetric content of abaca fiber, which, subsequently, increased to 11.8%. This proved that the increase and decrease in the CS of abaca-based HSFRC had a parabolic tendency.

According to the compressive strength of ramie–abaca HSFRC, the presence of fibers prevented and delayed cracks when the compression load was applied. When the load was increased and cracks occurred, these fibrous materials prevented and bridged the crack propagation and gap occurrences, respectively. This led to concrete destruction delay, increased compression load, and high compressive strength. However, when the fibers exceeded the optimum level, a roughly mixed composition was observed, leading to the appearance of fibrous concrete clumps. This was emphasized by the occurrence of a smaller flow speed than that of the concrete without fibers (Figures 10 and 11). The presence of these fibrous clumps also caused ineffective inhibition of crack emergence and propagation, leading to a reduction in compressive strength. This was, subsequently, prevented by providing a larger portion of superplasticizer to the concrete mix using a higher amount of fiber.

3.3. Flexural Strength

Figures 14 and 15 show the results of the flexural strength (FS) test of the HSFRC mixtures with and without CDE, using ramie and abaca fibers (RF and AF). These conditions indicated that FS increased with the addition of 0.3% RF and AF, although decreased under the provision of 0.45% volumetric content. Similar to the compressive strength, the increase and decrease in FS also had a parabolic tendency. Besides the parabolic trendlines, the bi-linear trendlines, of the relationship between flexural strength and fiber content, were also plotted in Figures 14 and 15.

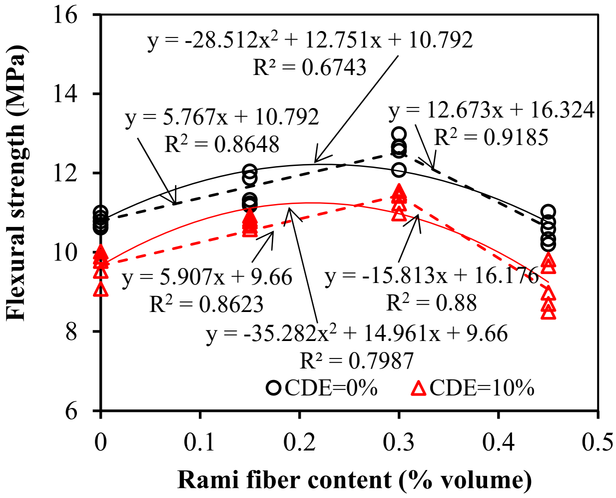

Figure 14. Flexural strength of HSFRC with ramie fiber.

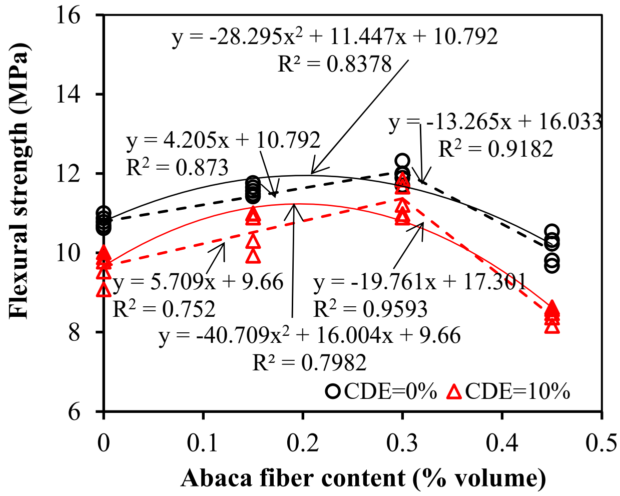

Figure 15. Flexural strength of HSFRC with abaca fiber.

Based on the addition of 0.3% RF, the flexural strength increased by 16.6% and 17.3% for the HSFRC without and with CDE, respectively. Meanwhile, the provision of 0.3% AF increased the FS of the HSFRC without and with CDE by 17.2% and 9.4%, respectively. Regarding the addition of 0.45% RF and AF, a decrease was observed in the flexural strength, although the values were almost similar to that of the non-fibrous concrete. Differing from the compressive strength estimations, the presence of CDE as a cement replacement significantly contributed to an increase in FS, regarding the addition of fiber.

In the flexural test, the beam used provided a positive bending moment, which caused compressed and tensile conditions at the top and bottom of the specimen, respectively. Since its tensile strength was very small compared to the CS, failure was observed for the bending moment due to tensile stress (TS). This indicated that the fracture process of concrete under flexural test was almost similar to that under tension. From these results, the presence of fibers effectively bridged and prevented the occurrences of cracks and cracking propagation, respectively. This caused a change in the brittleness of the concrete under flexural test toward a plastic behavior, subsequently, leading to increased FS and the non-occurrence of immediate failure.

In the simple and finite-element stress analyses of reinforced concrete, flexural strength (FS) is not often inputted as a separate quantity, although it was calculated as a function of compressive strength (CS). Similar to practical applications, only the CS is commonly tested, with the FS value calculated by the equation recommended by the building codes. According to ACI 318-19, the relationship between flexural (f_r) and compressive (f'_c) strengths recommended for normal-strength concrete is $f_r = 0.62\sqrt{f'_c}$ [88]. Meanwhile, ACI 363R-10 recommends the relationship for high-strength concrete as $f_r = 0.94\sqrt{f'_c}$ [1]. The recommended and presently-analyzed results are presented together in Figure 16. This proved that the flexural strength obtained in the present analysis was higher than that of the recommendations, indicating the effectiveness of using ramie and abaca fibers in increasing the FS of concrete. Based on the data analyzed in this study, the relationship can be written as $f_r = 1.19\sqrt{f'_c}$.

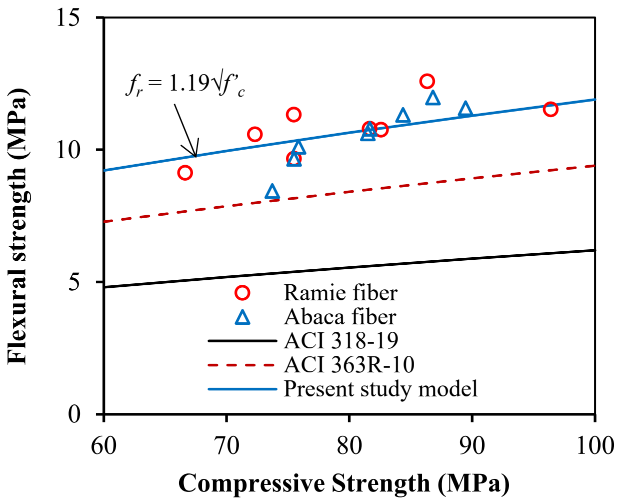

Figure 16. Relationship between flexural strength and compressive strength of FRHSC.

3.4. Splitting Tensile Strength

Figure 17 shows the splitting tensile strength (STS) test of the HSFRC with and without CDE, using ramie fiber (RF). This confirmed that the STS increased with higher RF application. Although the splitting tensile strength of the non-fibrous HSFRC with 10% CDE was lower than the type without CDE, its increase was still highly significant, due to the elevated volumetric content of the ramie fiber. This confirmed that the values of STS for the two mixtures were almost the same regarding the addition of 0.45% RF. In this process, the STS was increased by 24% and 31.8% in the HSFRC mixture without and with

CDE, respectively. As a function of the volumetric content of ramie fiber, the increase in splitting tensile strength was parabolic, with a decrease likely to occur for fiber additions above 0.45%.

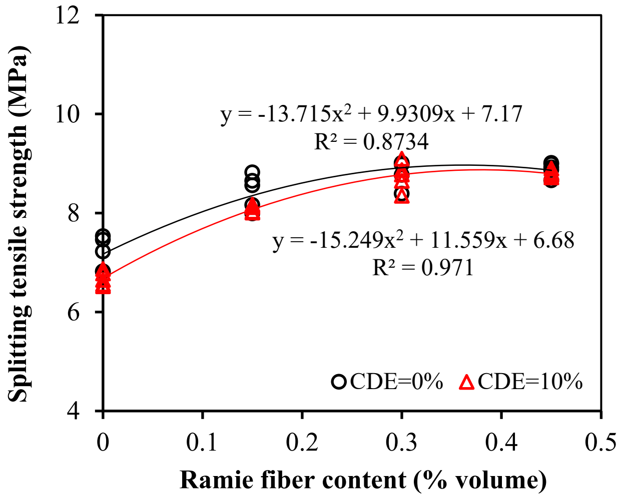

Figure 17. Splitting tensile strength of FRHSC with ramie fiber.

Figure 18 shows the splitting tensile strength test of the HSFRC with and without CDE, using abaca fiber (AF). For the mixture with AF, the STS increased and decreased for the 0.3% and 0.45% volumetric contents, respectively. However, the value was greater than the splitting tensile strength of non-fibrous concrete. This showed that the increase and decrease in the STS of HSFRC were parabolic. Based on the addition of 0.3% abaca fiber, the maximum splitting tensile strength was obtained, with an increase of 36.8% and 38.1% for the HSFRC without and with CDE, respectively. The improvement of splitting tensile strength for HSFRC with abaca fiber was higher than that with ramie fiber, which was due to the higher tensile strength of abaca fiber, compared to ramie fiber, as shown in Table 3. The splitting tensile strength of HSFRC with CDE was lower than that without CDE and this finding was in line with the finding reported in the previous study [10].

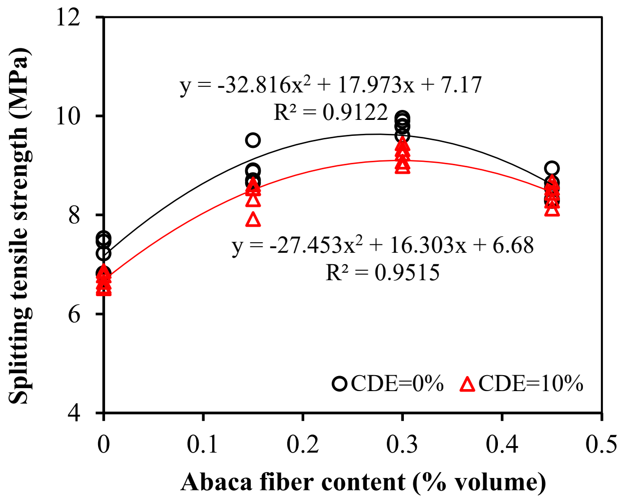

Figure 18. Splitting tensile strength of FRHSC with abaca fiber.

Concrete is a heterogeneous material consisting of aggregates, and cement paste, and an interface between both elements (cement paste and aggregates). This shows that the tensile strength of this material is not uniform. In this case, the tensile strength of concrete is considered to be normally distributed [89–91]. When a tensile load is excessively applied to concrete, crack occurrences are initially observed for the low-strength element [92]. These cracks, subsequently, propagate to other areas of slightly higher tensile strength when the applied load is increased, leading to brittle failure in the fracture process. These crack gaps and propagation are often bridged and prevented through the provision of fibers, leading to a change from brittleness to plastic behavior. This process causes the tensile strength of the concrete to increase, due to the presence of fibers.

Similar to FS (flexural strength), the splitting tensile strength of concrete is not practically tested. When required for behavioral analysis of reinforced concrete structures, its value is commonly considered in accordance with the equation recommended by building codes. According to ACI 318-19, the relationship between splitting tensile (f_{sp}) and compressive (f'_c) strengths recommended for normal-strength concrete is $f_{sp} = 0.56\sqrt{f'_c}$ [88]. Meanwhile, ACI 363R-10 recommends the relationship for high-strength concrete is $f_{sp} = 0.59\sqrt{f'_c}$ [1]. These recommended and presently-analyzed values were plotted together in Figure 19. This indicated that the presently-analyzed STS was higher than that of the recommendations, significantly proving the effectiveness of the ramie and abaca fibers in increasing the splitting tensile strength of concrete. Based on the data analyzed in this study, the relationship can be written as $f_{sp} = 0.93\sqrt{f'_c}$.

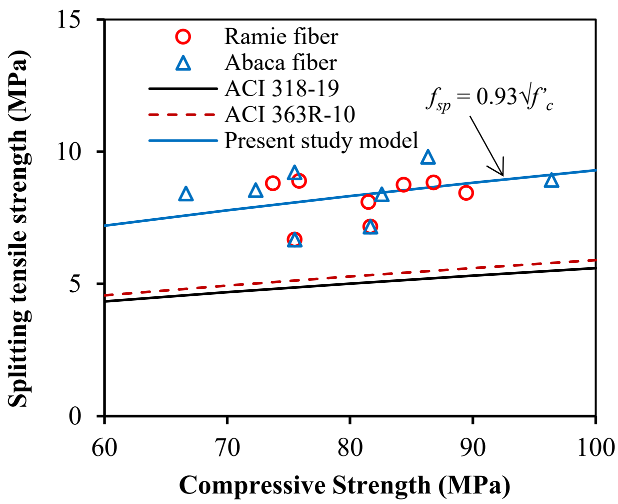

Figure 19. Relationship between splitting tensile strength and compressive strength of FRHSC.

3.5. Absorption

Figures 20 and 21 show the HSFRC absorption test with and without CDE, using ramie and abaca fibers. These conditions indicated that no effect was observed in the addition of fiber to the absorption of concrete, regarding the HSFRC mixture without CDE. Meanwhile, a slight increase was found in this absorption after adding both ramie and abaca fibers to the HSFRC with 10% CDE. All these absorption values were still < 5%, despite the results obtained, proving that they were sufficiently small for good durability. The absorption of concrete is often associated with the assimilation of surface water and chemicals, such as chloride, carbon dioxide, and sulfate, from the external environment through the pores. Smaller absorption values cause a lower possibility of these substances being assimilated into the concrete, subsequently leading to higher durability. Regarding Figures 20 and 21, the HSFRC with CDE had greater absorption than using only the OPC. This was due to the absorption value of 6.54% and the cellular nature of the CDE nanopores structure (Table 1 and Figure 2). These results were in line with a previous study, regarding the analysis of cement mortar with CDE [93].

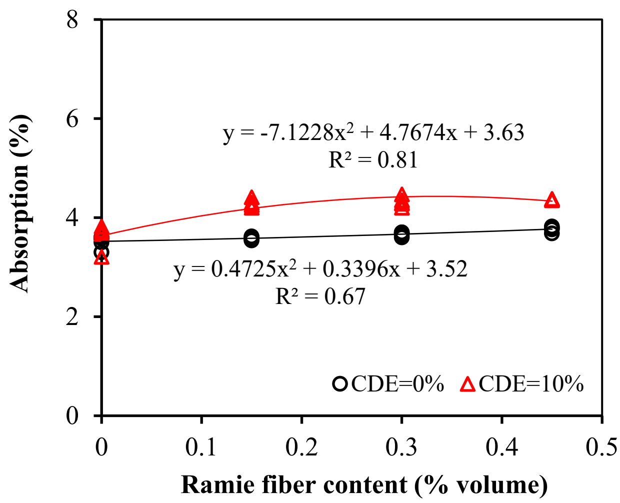

Figure 20. Absorption of FRHSC with ramie fiber.

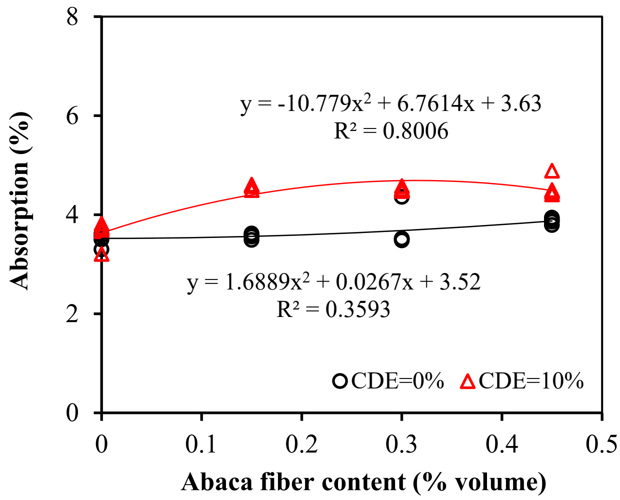

Figure 21. Absorption of FRHSC with abaca fiber.

Since ramie and abaca fibers are processed from plants, they should be renewed by growing more productive plantations. These fibers are sustainable materials, whose adoption often leads to a significant increase in mechanical properties. This shows that they can be used as alternatives to guarantee the production of sustainable fiber concrete. The numeric data for compressive strength, flexural strength, tensile strength, and absorption, together with average value, standard deviation (SD), and coefficient of variance (CV) are presented in Appendix A Tables A1–A4. Most of the data had a coefficient of variance of less than 5% which confirmed the reliability of the data presented in this study. It is important to note that this study only focused on the mechanical properties and absorption of concrete. The microstructures and pore distribution will be investigated in further study.

4. Conclusions

A total of 14 high-strength fiber-reinforced concrete (HSFRC) mixtures were prepared in this study, with two not using fiber and adopted as control composition. One of these mixtures only used Type-I Ordinary Portland Cement (OPC) as a binder, with the other using 10% calcined diatomaceous earth (CDE). Furthermore, 0.15%, 0.3%, and 0.45% of the concrete volume were added to the two mixtures, using ramie and abaca fibers. Based on the results, the following conclusions can be drawn:

1. The addition of ramie and abaca fibers (RF and AF) to the mixture of high-strength concrete reduced the flow speed of fresh HSFRC, which then, subsequently, decreased

with increasing fibrous volumetric content. The use of CDE as a cement substitute also reduced the flow speed of the fresh material.
2. The additions of RF and AF of 0.15% and 0.3% increased the compressive strength (CS) of HSFRC. For the 0.15% ramie fiber, the CS increased to 18% and 9.4% for the HSFRC without and with CDE, respectively. Meanwhile, the use of 0.15% and 0.3% abaca fiber increased CS to 9.6% and 11.8% for the mixtures without and with CDE, respectively.
3. The addition of ramie and abaca fibers up to 0.3% also increased the flexural strength (FS) of HSFRC. For RF, the FS increased to 16.6% and 17.3% for the HSFRC without and with CDE, respectively. However, the abaca fiber increased this strength to 17.2% and 9.4% for the mixtures without and with CDE, respectively.
4. Regarding the addition of RF and AF, the splitting tensile strength of HSFRC was also increased. This indicated that the largest increase for ramie fiber occurred at 0.45%, with the STS elevated to 24% and 31.8% for the HSFRC with and without CDE, respectively. Meanwhile, the largest increase for abaca fiber occurred at 0.3%, with the STS elevated to 36.8% and 38.1% for the mixtures without and with CDE.
5. Using the ramie and abaca fibers, the elevations in the absorption value of the HSFRC without and with CDE were insignificant and significant, respectively. This indicated that the mixtures with CDE had greater values, which were all below 5%.
6. Since in this paper only the mechanical properties of HSFRC with ramie and abaca fibers were studied, it is recommended to conduct further study on the micro-structures and pore distribution of HSFRC with the same fibers.

Author Contributions: Conceptualization, M.H. and T.S.; methodology, M.H., T.S. and Z.A.; investigation, M.H., M.J., Z.A. and A.M.; validation, M.H., T.S. and M.J.; resources, M.H.; writing—original draft preparation, M.H., Z.A. and A.M.; writing—review and editing, M.H.; supervision, T.S. All authors have read and agreed to the published version of the manuscript.

Funding: This research was funded by the Directorate General of Higher Education, Research, and Technology, Ministry of Education, Culture, Research, and Technology, Republic of Indonesia (contract number: 145/E5/PG.02.00.PT/2022) and the Research and Community Service Center of Universitas Syiah Kuala (contract number: 47/UN11.2.1/PT.01.03/DPRM/2022).

Institutional Review Board Statement: Not applicable.

Informed Consent Statement: Not applicable.

Data Availability Statement: The data of this research is available upon request to the first author.

Acknowledgments: The authors are grateful to Mahlil, Eva Ayudya Maharani, Maulana Alief Ghifari, and M. Nasir for the assistance provided in the experimental activities needed for data collection.

Conflicts of Interest: The authors declare no conflict of interest.

Appendix A

Table A1. Compressive Strength Data.

Mixture	CDE Content (% Binder Weight)	Fiber Type	Fiber Content (% Volume)	Compressive Strength (MPa)							CV (%)
				#1	#2	#3	#4	#5	Average	SD	
HSC00F00	0	-	0	90.53	74.84	79.99	80.56	82.34	81.65	5.69	6.97
HSC10F00	10	-	0	80.77	74.14	70.00	75.67	76.86	75.49	3.93	5.20
HSC00RF15	0	RF	0.15	94.17	103.86	88.18	100.20	95.63	96.41	5.98	6.21
HSC00RF30	0	RF	0.30	88.00	87.00	86.56	83.65	86.54	86.35	1.62	1.88
HSC00RF45	0	RF	0.45	73.50	73.99	67.27	75.22	71.56	72.31	3.11	4.30
HSC00AF15	0	AF	0.15	85.91	93.24	88.62	90.00	89.56	89.47	2.64	2.95
HSC00AF30	0	AF	0.30	91.02	85.00	86.00	86.34	85.67	86.81	2.41	2.77
HSC00AF45	0	AF	0.45	80.54	72.89	71.87	76.34	77.62	75.85	3.53	4.66
HSC10RF15	10	RF	0.15	82.60	82.09	80.33	83.34	84.56	82.58	1.57	1.90
HSC10RF30	10	RF	0.30	73.57	75.52	76.00	74.31	78.00	75.48	1.71	2.26
HSC10RF45	10	RF	0.45	59.68	71.01	63.91	69.90	68.67	66.63	4.74	7.11
HSC10AF15	10	AF	0.15	78.17	82.65	78.12	85.23	83.33	81.50	3.21	3.93
HSC10AF30	10	AF	0.30	83.69	85.00	82.16	86.65	84.32	84.36	1.65	1.96
HSC10AF45	10	AF	0.45	69.98	69.58	79.36	75.34	74.35	73.72	4.06	5.51

Table A2. Flexural Strength Data.

Mixture	CDE Content (% Binder Weight)	Fiber Type	Fiber Content (% Volume)	Flexural Strength (MPa)							CV (%)
				#1	#2	#3	#4	#5	Average	SD	
HSC00F00	0	-	0	10.62	10.69	11.00	10.78	10.87	10.79	0.15	1.39
HSC10F00	10	-	0	9.53	9.08	10.02	9.89	9.78	9.66	0.37	3.84
HSC00RF15	0	RF	0.15	11.18	12.04	11.23	11.32	11.87	11.53	0.40	3.45
HSC00RF30	0	RF	0.30	12.56	12.65	12.67	12.07	12.98	12.59	0.33	2.62
HSC00RF45	0	RF	0.45	11.02	10.58	10.20	10.33	10.76	10.58	0.33	3.11
HSC00AF15	0	AF	0.15	11.65	11.42	11.76	11.56	11.48	11.57	0.14	1.17
HSC00AF30	0	AF	0.30	11.70	12.00	11.98	12.32	11.89	11.98	0.22	1.88
HSC00AF45	0	AF	0.45	9.81	9.67	10.23	10.54	10.32	10.11	0.36	3.59
HSC10RF15	10	RF	0.15	10.67	10.92	10.83	10.58	10.78	10.76	0.13	1.24
HSC10RF30	10	RF	0.30	10.98	11.45	11.23	11.55	11.42	11.33	0.23	1.99
HSC10RF45	10	RF	0.45	9.82	8.70	8.50	8.98	9.65	9.13	0.58	6.36
HSC10AF15	10	AF	0.15	9.93	10.30	10.99	11.00	10.89	10.62	0.48	4.55
HSC10AF30	10	AF	0.30	11.21	11.67	11.85	10.98	10.89	11.32	0.42	3.74
HSC10AF45	10	AF	0.45	8.63	8.58	8.16	8.37	8.48	8.44	0.19	2.22

Table A3. Splitting Tensile Strength Data.

Mixture	CDE Content (% Binder Weight)	Fiber Type	Fiber Content (% Volume)	Splitting Tensile Strength (MPa)							CV (%)
				#1	#2	#3	#4	#5	Average	SD	
HSC00F00	0	-	0	6.81	6.82	7.46	7.22	7.53	7.17	0.34	4.77
HSC10F00	10	-	0	6.87	6.56	6.52	6.78	6.65	6.68	0.15	2.21
HSC00RF15	0	RF	0.15	8.82	7.99	8.16	8.65	8.56	8.44	0.35	4.12
HSC00RF30	0	RF	0.30	8.39	8.77	9.01	9.00	8.98	8.83	0.27	3.00
HSC00RF45	0	RF	0.45	8.92	8.66	9.01	8.99	8.87	8.89	0.14	1.58
HSC00AF15	0	AF	0.15	8.70	9.51	8.65	8.88	8.90	8.93	0.34	3.84
HSC00AF30	0	AF	0.30	9.60	9.78	9.80	9.90	9.96	9.81	0.14	1.40
HSC00AF45	0	AF	0.45	8.32	8.94	8.28	8.65	8.54	8.55	0.27	3.14
HSC10RF15	10	RF	0.15	8.17	8.01	8.03	8.15	8.12	8.10	0.07	0.89
HSC10RF30	10	RF	0.30	9.10	8.65	8.35	8.78	8.87	8.75	0.28	3.17
HSC10RF45	10	RF	0.45	8.90	8.77	8.72	8.80	8.82	8.80	0.07	0.76
HSC10AF15	10	AF	0.15	8.55	8.54	7.92	8.32	8.62	8.39	0.29	3.41
HSC10AF30	10	AF	0.30	8.99	9.08	9.24	9.33	9.45	9.22	0.19	2.01
HSC10AF45	10	AF	0.45	8.45	8.13	8.55	8.67	8.29	8.42	0.21	2.53

Table A4. Absorption Data.

Mixture	CDE Content (% Binder Weight)	Fiber Type	Fiber Content (% Volume)	Absorption (%)							CV (%)
				#1	#2	#3	#4	#5	Average	SD	
HSC00F00	0	-	0	3.61	3.58	3.30	3.59	3.50	3.52	0.13	3.63
HSC10F00	10	-	0	3.21	3.72	3.82	3.75	3.67	3.63	0.24	6.69
HSC00RF15	0	RF	0.15	3.62	3.54	3.56	3.60	3.58	3.58	0.03	0.88
HSC00RF30	0	RF	0.30	3.60	3.70	3.70	3.65	3.68	3.67	0.04	1.15
HSC00RF45	0	RF	0.45	3.76	3.82	3.68	3.80	3.78	3.77	0.05	1.43
HSC00AF15	0	AF	0.15	3.62	3.49	3.56	3.58	3.59	3.57	0.05	1.36
HSC00AF30	0	AF	0.30	4.36	3.48	3.51	3.50	3.52	3.67	0.38	10.45
HSC00AF45	0	AF	0.45	3.91	3.79	3.94	3.88	3.86	3.88	0.06	1.47
HSC10RF15	10	RF	0.15	4.41	4.20	4.26	4.25	4.30	4.28	0.08	1.84
HSC10RF30	10	RF	0.30	4.47	4.20	4.35	4.30	4.28	4.32	0.10	2.31
HSC10RF45	10	RF	0.45	4.37	4.36	4.37	4.35	4.38	4.37	0.01	0.26
HSC10AF15	10	AF	0.15	4.58	4.60	4.61	4.50	4.59	4.58	0.04	0.96
HSC10AF30	10	AF	0.30	4.58	4.48	4.52	4.50	4.49	4.51	0.04	0.88
HSC10AF45	10	AF	0.45	4.89	4.48	4.41	4.46	4.50	4.55	0.19	4.27

References

1. *ACI 363-10: Report on High-Strength Concrete*; American Concrete Institute: Farmington Hills, MI, USA, 2010.
2. Wang, P.; Xie, M.; Liu, L. Studi on eraly shrinkage and mechanical properties of concrete with various cementitious materials. *Buildings* **2022**, *12*, 1543. [CrossRef]
3. Hakeem, I.Y.; Althoey, F.; Hosen, A. Mechanical and durability performance of ultra-high-performance concrete incorporating SCMs. *Constr. Build. Mater.* **2022**, *359*, 129430. [CrossRef]
4. Ali, T.; Buller, A.S.; Abro, F.R.; Ahmed, Z.; Shabbir, S.; Lashari, A.R.; Hussain, G. Investigation on mechanical and durability properties of concrete mixed with silica fume as cementitious material and coal buttom ash as fine aggregate replacement material. *Buildings* **2022**, *12*, 44. [CrossRef]
5. Shao, J.; Gao, J.; Zhao, Y.; Chen, X. Study on the pozzolanic reaction of clay brick powder in blended cement pastes. *Constr. Build. Mater.* **2019**, *213*, 209–215. [CrossRef]
6. Balasubramaniam, T.; Stephen, S.J. Influence of industrial wastes on the mechanical and durability characteristics of high strength concrete. *Constr. Build. Mater.* **2022**, *317*, 126202. [CrossRef]
7. Sosa, I.; Thomas, C.; Polanco, J.A.; Setién, J.; Sainz-Aja, J.A.; Tamayo, P. Durability of high-performance self-compacting concrete using electric arc furnace slag aggregate and cupola slag powder. *Cem. Concr. Compos.* **2022**, *127*, 104399. [CrossRef]
8. Sadrolodabaee, P.; Claramunt, J.; Ardanuy, M.; de la Fuente, A. Effect of accelerated aging and silica fume addition on the mechanical and microstructural properties of hybrid textile waste-flax fabric-reinforced cement composites. *Cem. Concr. Compos.* **2023**, *135*, 104829. [CrossRef]
9. Sadrmomtazi, A.; Tahmouresi, B.; Khoshkbijari, R.K. Effect of fly ash and silica fume on transition zone, pore structure and permeability of concrete. *Mag. Concr. Res.* **2018**, *70*, 519–532. [CrossRef]
10. Hamou, A.T.; Petrov, N.; Luke, K. Properties of concrete containing diatomaceous earth. *ACI Mater. J.* **2003**, *100*, 73–78.
11. Hasan, M.; Muyasir, A.; Saidi, T.; Husaini; Azzahra, R. Properties of high strength concrete with calcined diatomaceous earth as cement replacement under compression. *Defect Diffus. Forum* **2020**, *402*, 7–13. [CrossRef]
12. Hasan, M.; Riski, D.D.R.; Saidi, T.; Husaini; Rahman, P.N. Flexural and splitting tensile strength of high strength concrete with diatomite micro particles as mineral additive. *Defect Diffus. Forum* **2020**, *402*, 50–55. [CrossRef]
13. *ASTM C618-19*; Standard Specification for Coal Fly Ash and Raw or Calcined Natural Pozzolan for Use in Concrete. ASTM International: West Conshohocken, PA, USA, 2019.
14. Soroushian, P.; Tlili, A.; Alhozaimy, A.; Khan, A. Development and characterization of hybrid polyethylene-fibre-reinforced cement composites. *Constr. Build. Mater.* **1993**, *7*, 221–229. [CrossRef]
15. Komloš, K.; Babál, B.; Nürnbergerová, T. Hybrid fibre-reinforced concrete under repeated loading. *Nucl. Eng. Des.* **1995**, *156*, 195–200. [CrossRef]
16. Zollo, R.F. Fiber-reinforced concrete: An overview after 30 years of development. *Cem. Concr. Compos.* **1997**, *19*, 107–122. [CrossRef]
17. Dushimimana, A.; Niyonsenga, A.A.; Nzamurambaho, F. A review on strength development of high performance concrete. *Constr. Build. Mater.* **2021**, *307*, 124865. [CrossRef]
18. Nikbin, I.M.; Dezhampanah, S.; Charkhtab, S.; Mehdipour, S.; Shahvareh, I.; Ebrahimi, M.; Pournasir, A.; Pourghorban, H. Life cycle assessment and mechanical properties of high strength steel fiber reinforced concrete containing waste PET bottle. *Constr. Build. Mater.* **2022**, *337*, 127553. [CrossRef]
19. Yao, X.; Pei, Z.; Zheng, H.; Guan, Q.; Wang, F.; Wang, S.; Ji, Y. Review of mechanical and temperature properties of fiber reinforced recycled aggregate concrete. *Buildings* **2022**, *12*, 1224. [CrossRef]

20. Moradllo, M.K.; Qiao, C.; Isgor, B.; Reese, S.; Weiss, W.J. Relating formation factor of concrete to water absorption. *ACI Mater. J.* **2018**, *115*, 887–898. [CrossRef]
21. Xie, T.; Visintin, P. A unified approach for mix design of concrete containing supplementary cementitious materials based on reactivity moduli. *J. Clean. Prod.* **2018**, *203*, 68–82. [CrossRef]
22. Xie, T.; Fang, C.; Ali, M.M.; Visintin, P. Characterizations of autogenous and drying shrinkage of ultra-high performance concrete (UHPC): An experimental study. *Cem. Concr. Compos.* **2018**, *91*, 156–173. [CrossRef]
23. Song, P.S.; Hwang, S. Mechanical properties of high-strength steel fiber reinforced concrete. *Constr. Build. Mater.* **2004**, *18*, 669–673. [CrossRef]
24. Silva, R.V.; De Brito, J.; Dhir, R.K. Tensile strength behaviour of recycled aggregate concrete. *Constr. Build. Mater.* **2015**, *83*, 108–118. [CrossRef]
25. Shen, D.; Liu, X.; Li, Q.; Sun, L.; Wang, W. Early-age behavior and cracking resistance of high-strength concrete reinforced with Dramix 3D steel fiber. *Constr. Build. Mater.* **2019**, *196*, 307–316. [CrossRef]
26. Usman, M.; Farooq, S.H.; Umair, M.; Hanif, A. Axial compressive behavior of confined steel fiber reinforced high strength concrete. *Constr. Build. Mater.* **2020**, *230*, 117043. [CrossRef]
27. Cui, K.; Chang, J.; Sabri, M.M.S.; Huang, J. Toughness, reinforcing mechanism, and durability of hybrid steel fiber reinforced sulfoaluminate cement composites. *Buildings* **2022**, *12*, 1243. [CrossRef]
28. Vafaei, D.; Ma, X.; Hassanli, R.; Duan, J.; Zhuge, Y. Microstructural behaviour and shrinkage properties of high-strength fiber-reinforced seawater sea-sand concrete. *Constr. Build. Mater.* **2022**, *320*, 126222. [CrossRef]
29. Shen, D.; Wena, C.; Kang, J.; Shi, H.; Xu, Z. Early-age stress relaxation and cracking potential of high-strength concrete reinforced with Barchip fiber. *Constr. Build. Mater.* **2020**, *258*, 119538. [CrossRef]
30. Li, K.F.; Yang, C.Q.; Huang, W.; Zhao, Y.B.; Wang, Y.; Pan, Y.; Xub, F. Effects of hybrid fibers on workability, mechanical, and time-dependent properties of high strength fiber-reinforced self-consolidating concrete. *Constr. Build. Mater.* **2021**, *277*, 122325. [CrossRef]
31. Shoaib, S.; El-Maaddawy, T.; El-Hassan, H.; El-Ariss, B.; Alsalami, M. Fresh and hardened properties of concrete reinforced with basalt macro-fibers. *Buildings* **2022**, *12*, 1136. [CrossRef]
32. Akeed, M.H.; Qaidi, S.; Ahmed, H.U.; Faraj, R.H.; Mohammed, A.S.; Emad, W.; Tayeh, B.A.; Azevedo, A.R.G. Ultra-high-performance fiber-reinforced concrete. Part IV: Durability properties, cost assessment, applications, and challenges. *Case Stud. Constr. Mater.* **2022**, *17*, e01271. [CrossRef]
33. Lee, M.G.; Wang, W.C.; Wang, Y.C.; Hsieh, Y.C.; Lin, Y.C. Mechanical properties of high-strength pervious concrete with steel fiber or glass fiber. *Buildings* **2022**, *12*, 620. [CrossRef]
34. Wang, L.; Zeng, X.; Li, Y.; Yang, H.; Tang, S. Influences of MgO and PVA fiber on the abrasion and cracking resistance, pore structure and fractal features of hydraulic concrete. *Fractal Fract.* **2022**, *6*, 674. [CrossRef]
35. Wang, L.; Guo, F.; Yang, H.; Wang, Y.; Tang, S. Comparison of fly ash, PVA fiber, MGO and shrinkage-reducing admixture on the frost resistance of face slab concrete via pore structural and fractal analysis. *Fractal* **2021**, *29*, 2140002. [CrossRef]
36. Wang, L.; He, T.; Zhou, Y.; Tang, S.; Tan, J.; Liu, Z.; Su, J. The influence of fiber type and length on the cracking resistance, durability and pore structure of face slab concrete. *Constr. Build. Mater.* **2021**, *282*, 122706. [CrossRef]
37. Mínguez, J.; González, D.C.; Vicente, M.A. Fiber geometrical parameters of fiber-reinforced high strength concrete and their influence on the residual post-peak flexural tensile strength. *Constr. Build. Mater.* **2018**, *168*, 906–922. [CrossRef]
38. Abid, S.R.; Abbass, A.A.; Murali, G.; Al-Sarray, M.L.J.; Nader, I.A.; Ali, S.H. Post-high-temperature exposure repeated impact response of steel-fiber-reinforced concrete. *Buildings* **2022**, *12*, 1364. [CrossRef]
39. Ding, X.; Li, C.; Zhao, M.; Wang, H.; Dang, J.; Zhao, S. Bond performance of hook-end steel fiber to the mortars cured for 360 days. *Buildings* **2022**, *12*, 1424. [CrossRef]
40. He, J.; Chen, W.; Zhang, B.; Yu, J.; Liu, H. The mechanical properties and damage evolution of UHPC reinforced with glass fibers and high-performance polypropylene fibers. *Materials* **2021**, *14*, 2455. [CrossRef]
41. Ahmad, J.; González-Lezcano, R.A.; Majdi, A.; Kahla, N.B.; Deifalla, A.F.; El-Shorbagy, M.A. Glass fibers reinforced concrete: Overview on mechanical, durability and microstructure analysis. *Materials* **2022**, *15*, 5111. [CrossRef]
42. Hussaina, I.; Alib, B.; Akhtarb, T.; Jameela, M.S.; Raza, S.S. Comparison of mechanical properties of concrete and design thickness of pavement with different types of fiber-reinforcements (steel, glass, and polypropylene). *Case Stud. Constr. Mater.* **2020**, *13*, e00429. [CrossRef]
43. Cui, K.; Liang, K.; Chang, J.; Lau, D. Investigation of the macro performance, mechanism, and durability of multiscale steel fiber reinforced low-carbon ecological UHPC. *Constr. Build. Mater.* **2022**, *327*, 126921. [CrossRef]
44. Jhatial, A.A.; Goh, W.I.; Mastoi, A.K.; Traore, A.F.; Oad, M. Environmental assessment and mechanical properties of polypropylene fibres reinforced ternary binder foamed concrete. *Environ. Sci. Pollut. Res.* **2022**, *29*, 2985–3007. [CrossRef] [PubMed]
45. Kim, S.W.; Jang, S.J.; Kang, D.H.; Ahn, K.L.; Yun, H.D. Mechanical properties and eco-efficiency of steel fiber reinforced alkali-activated slag concrete. *Materials* **2015**, *8*, 7309–7321. [CrossRef] [PubMed]
46. Hu, P.; Li, Y.; Zhang, X.; Guo, Z.; Zhang, P. CO_2 emission from container glass in China, and emission reduction strategy analysis. *Carbon Manag.* **2018**, *9*, 303–310. [CrossRef]
47. Hamdaoui, O.; Limam, O.; Ibos, L.; Mazioud, A. Thermal and mechanical properties of hardened cement paste reinforced with Posidonia-Oceanica natural fibers. *Constr. Build. Mater.* **2021**, *269*, 121339. [CrossRef]

48. Stapper, J.L.; Gauvin, F.; Brouwers, H.J.H. Influence of short-term degradation on coir in natural fibre-cement composites. *Constr. Build. Mater.* **2021**, *306*, 124906. [CrossRef]
49. Choi, H.; Choi, Y.C. Setting characteristics of natural cellulose fiber reinforced cement composite. *Constr. Build. Mater.* **2021**, *271*, 121910. [CrossRef]
50. Suwan, T.; Maichin, P.; Fan, M.; Jitsangiam, P.; Tangchirapat, W.; Chindaprasirt, P. Influence of alkalinity on self-treatment process of natural fiber and properties of its geopolymeric composites. *Constr. Build. Mater.* **2022**, *316*, 125817. [CrossRef]
51. Sadrolodabaee, P.; Claramunt, J.; Ardanuy, M.; de la Fuente, A. A textile waste fiber-reinforced cement composite: Comparison between short random fiber and textile reinforcement. *Materials* **2021**, *14*, 3742. [CrossRef]
52. Ardanuy, M.; Claramunt, J.; Filho, R.D.T. Cellulosic fiber reinforced cement-based composites: A review of recent research. *Constr. Build. Mater.* **2015**, *79*, 115–128. [CrossRef]
53. Gholampour, A.; Danish, A.; Ozbakkaloglu, T.; Yeon, J.H.; Gencel, O. Mechanical and durability properties of natural fiber-reinforced geopolymers containing lead smelter slag and waste glass sand. *Constr. Build. Mater.* **2022**, *352*, 129043. [CrossRef]
54. More, F.M.D.S.; Subramanian, S.S. Impact of fibres on the mechanical and durable behaviour of fibre-reinforced concrete. *Buildings* **2022**, *12*, 1436. [CrossRef]
55. Katman, H.Y.B.; Khai, W.J.; Bheel, N.; Kırgız, M.S.; Kumar, A.; Benjeddou, O. Fabrication and characterization of cement-based hybrid concrete containing coir fiber for advancing concrete construction. *Buildings* **2022**, *12*, 1450. [CrossRef]
56. Parlato, M.C.M.; Cuomo, M.; Porto, S.M.C. Natural fibers reinforcement for earthen building components: Mechanical performances of a low quality sheep wool ("Valle del Belice" sheep). *Constr. Build. Mater.* **2022**, *326*, 126855. [CrossRef]
57. Habibie, S.; Suhendra, N.; Setiawan, B.A.; Hamzah, M.; Aisah, N.; Fitriani, D.A.; Tasomara, R.; Anggaravidya, M. Prospect of ramie fiber development in Indonesia and manufacturing of ramie fiber textile-based composites for industrial needs, an overview. *Int. J. Compos. Mater.* **2021**, *11*, 43–53. [CrossRef]
58. Jamilah, U.L.; Sujito. The improvement of ramie fiber properties as composite materials using alkalization treatment: NaOH concentration. *J. Sci. Mater. Indo.* **2021**, *22*, 62–70. [CrossRef]
59. Li, Z.; Zou, Y.; Li, S.; Guo, Y.; Zeng, X.; Zhu, J.; Zhang, S. Direct extraction of fibre from a ramie bark. *J. Eng. Fibers Fabrics.* **2020**, *15*, 1–7. [CrossRef]
60. Jose, S.; Rajna, S.; Ghosh, P. Ramie fiber processing and value addition. *Asian J. Textile.* **2017**, *7*, 1–9. [CrossRef]
61. Sathish, T.; Palani, K.; Natrayan, L.; Merneedi, A.; De Poures, M.V.; Singaravelu, D.K. Shinthesis and characterization of polypropylene/ramie fiber with hemp fiber and coir fiber natural biopolymer composite for biomedical application. *Int. J. Polym. Sci.* **2021**, *2021*, 2462878. [CrossRef]
62. Shibata, M.; Ozawa, K.; Teramoto, N.; Yosomiya, R.; Takeishi, H. Biocomposites made from short abaca fiber and biodegradable polyesters. *Macromol. Mater. Eng.* **2003**, *288*, 35–43. [CrossRef]
63. Barba, B.J.D.; Madrid, J.F.; Penaloza, D.P., Jr. A review of abaca fiber-reinforced polymer composites: Different modes of preparation and their applications. *J. Chil. Chem. Soc.* **2020**, *65*, 4919–4924. [CrossRef]
64. Alshgari, R.A.; Hemalatha, N.; Suryavanshi, A.; Prasad, D.V.S.S.S.V.; Subalakshmi, R.; Abirami, M.; Amudha, M.J.R.; Wabaidur, S.M.; Islam, M.A.; Christopher, D. Investigation on physical and mechanical properties of abaca fiber composites using filament winding. *Adv. Polym. Technol.* **2022**, *2022*, 5000547. [CrossRef]
65. Saidi, T.; Hasan, M.; Amalia, Z.; Iqbal, M. Behaviour analysis of strengthened-RC beam with natural fiber reinforced polymer (NFRP) based on abaca fiber by using finite element method. *Aceh Int. J. Sci. Technol.* **2022**, *11*, 155–164. [CrossRef]
66. Saidi, T.; Hasan, M.; Amalia, Z. Tensile strength of natural fiber in different types of matrix. *Aceh Int. J. Sci. Technol.* **2022**, *11*, 136–144. [CrossRef]
67. Malenab, R.A.J.; Ngo, J.P.S.; Promentilla, M.A.B. Chemical treatment of waste abaca for natural fiber-reinforced geopolymer composite. *Materials* **2017**, *10*, 579. [CrossRef] [PubMed]
68. Valášek, P.; Müller, M.; Šleger, V.; Kolář, V.; Hromasová, M.; D'Amato, R.; Ruggiero, A. Influence of alkali treatment on the microstructure and mechanical properties of coir and abaca fibers. *Materials* **2021**, *14*, 2636. [CrossRef]
69. *ASTM C150/C150M-22*; Standard Specification for Portland Cement. ASTM International: West Conshohocken, PA, USA, 2022.
70. Hasan, M.; Saidi, T.; Muyasir, A.; Alkhaly, Y.R.; Muslimsyah, M. Characteristics of calcined diatomaceous earth from Aceh Besar District–Indonesia as cementitious binder. *IOP Conf. Ser. Mater. Sci. Eng.* **2020**, *933*, 012008. [CrossRef]
71. Hasan, M.; Saidi, T. Properties of blended cement paste with diatomite from Aceh Province Indonesia. *IOP Conf. Ser. Mater. Sci. Eng.* **2020**, *796*, 012034. [CrossRef]
72. Hasan, M.; Saidi, T.; Husaini, H. Properties and microstructure of composite cement paste with diatomaceous earth powder (DEP) from Aceh Besar district–Indonesia. *Asia-Pacific J. Sci Technol.* **2022**, *27*, APST-27-01-03. [CrossRef]
73. *ASTM C33/C33M-18*; Standard Specification for Concrete Aggregates. ASTM International: West Conshohocken, PA, USA, 2018.
74. *ASTM D3822/D3822M-14*; Standard Test Method for Tensile Properties of Single Textile Fibers. ASTM International: West Conshohocken, PA, USA, 2020.
75. *ASTM C1602/C1602M-22*; Standard Specification for Mixing Water Used in the Production of Hydraulic Cement Concrete. ASTM International: West Conshohocken, PA, USA, 2022.
76. *ACI 211.4R-93*; Guide for Selecting Proportions for High-Strength Concrete with Portland Cement and Fly Ash. American Concrete Institute: Farmington Hills, MI, USA, 1998.

77. *ASTM C39/C39M-21*; Standard Test Method for Compressive Strength of Cylindrical Concrete Specimens. ASTM International: West Conshohocken, PA, USA, 2021.
78. *ASTM C78/C78M-22*; Standard Test Method for Flexural Strength of Concrete (Using Simple Beam with Third-Point Loading). ASTM International: West Conshohocken, PA, USA, 2022.
79. *ASTM C496/C496M-17*; Standard Test Method for Splitting Tensile Strength of Cylindrical Concrete Specimens. ASTM International: West Conshohocken, PA, USA, 2017.
80. *ASTM C642-21*; Standard Test Method for Density, Absorption, and Voids in Hardened Concrete. ASTM International: West Conshohocken, PA, USA, 2021.
81. Özcan, F.; Emin Koç, M. Influence of ground pumice on compressive strength and air content of both non-air and air entrained concrete in fresh and hardened state. *Constr. Build. Mater.* **2018**, *187*, 382–393. [CrossRef]
82. Vimonsatit, V.; Chindaprasirt, P.; Ruangsiriyakul, S.; Sata, V. Influence of fly ash fineness on water requirement and shrinkage of blended cement mortars. *KKU Eng. J.* **2015**, *42*, 311–316. [CrossRef]
83. Wu, Z.; Shi, C.; Khayat, K.H.; Wan, S. Effects of different nanomaterials on hardening and performance of ultra-high strength concrete (UHSC). *Cem. Concr. Compos.* **2016**, *70*, 24–34. [CrossRef]
84. Grünewald, S. *Performance-Based Design of Self-Compacting Fibre Reinforced Concrete*; Delft University of Technology: Delft, the Netherlands, 2004.
85. Edgington, J.; Hannant, D.J.; Williams, R.I.T. *Steel Fibre Reinforced Concrete, Fibre Reinforced Materials*; The Construction Press: Lancaster, UK; pp. 112–128.
86. Yu, R.; Tang, P.; Spiesz, P.; Brouwers, H.J.H. A study of multiple effects of nano-silica and hybrid fibres on the properties of ultra-high performance fibre reinforced concrete (UHPFRC) incorporating waste bottom ash (WBA). *Constr. Build. Mater.* **2014**, *60*, 98–110. [CrossRef]
87. Yu, R.; Spiesz, P.; Brouwers, H.J.H. Mix design and properties assessment of ultra-high performance fibre reinforced concrete (UHPFRC). *Cem. Concr. Res.* **2014**, *56*, 29–39. [CrossRef]
88. *ACI 318-19. Building Code Requirements for Structural Concrete*; American Concrete Institute: Farmington Hills, MI, USA, 2019.
89. Nagai, K.; Sato, Y.; Ueda, T. Mesoscopic simulation of failure of mortar and concrete by 2D RMSM. *J. Adv. Concr. Technol.* **2004**, *2*, 359–374. [CrossRef]
90. Hasan, M.; Okuyama, H.; Sato, Y.; Ueda, T. Stress-strain model of concrete damaged by freezing and thawing cycles. *J. Adv. Concr. Technol.* **2004**, *2*, 89–99. [CrossRef]
91. Nagai, K.; Sato, Y.; Ueda, T. Mesoscopic simulation of failure of mortar and concrete by 3D RMSM. *J. Adv. Concr. Technol.* **2005**, *3*, 385–402. [CrossRef]
92. Ueda, T.; Hasan, M.; Nagai, K.; Sato, Y.; Wang, L. Mesoscale simulation of influence of frost damage on mechanical properties of concrete. *J. Mater. Civ. Eng.* **2009**, *21*, 244–252. [CrossRef]
93. Saidi, T.; Hasan, M. The effect of partial replacement of cement with diatomaceous earth (DE) on the compressive strength and absorption of mortar. *J. King Saud Univ. Eng. Sci.* **2022**, *34*, 250–259. [CrossRef]